NAD+ repletion improves muscle function in muscular dystrophy and counters global PARylation

Ryu, Dongryeol; Zhang, Hongbo; Ropelle, Eduardo R; Sorrentino, Vincenzo; Mázala, Davi A G; Mouchiroud, Laurent; Marshall, Philip L; Campbell, Matthew D; Ali, Amir Safi; Knowels, Gary M; Bellemin, Stéphanie; Iyer, Shama R; Wang, Xu; Gariani, Karim [**and 10 more**]

How to cite

RYU, Dongryeol et al. NAD+ repletion improves muscle function in muscular dystrophy and counters global PARylation. In: Science Translational Medicine, 2016, vol. 8, n° 361, p. 361ra139. doi: 10.1126/scitranslmed.aaf5504

This publication URL: https://archive-ouverte.unige.ch/unige:143006

Publication DOI: 10.1126/scitranslmed.aaf5504

AGING

NAD+ repletion improves mitochondrial and stem cell function and enhances life span in mice

Hongbo Zhang,[1] Dongryeol Ryu,[1] Yibo Wu,[2] Karim Gariani,[1] Xu Wang,[1] Peiling Luan,[1] Davide D'Amico,[1] Eduardo R. Ropelle,[1,3] Matthias P. Lutolf,[4] Ruedi Aebersold,[2,5] Kristina Schoonjans,[6] Keir J. Menzies,[1,7]* Johan Auwerx[1]*

Adult stem cells (SCs) are essential for tissue maintenance and regeneration yet are susceptible to senescence during aging. We demonstrate the importance of the amount of the oxidized form of cellular nicotinamide adenine dinucleotide (NAD^+) and its effect on mitochondrial activity as a pivotal switch to modulate muscle SC (MuSC) senescence. Treatment with the NAD^+ precursor nicotinamide riboside (NR) induced the mitochondrial unfolded protein response and synthesis of prohibitin proteins, and this rejuvenated MuSCs in aged mice. NR also prevented MuSC senescence in the *mdx* (C57BL/10ScSn-*Dmd*^{mdx}/J) mouse model of muscular dystrophy. We furthermore demonstrate that NR delays senescence of neural SCs and melanocyte SCs and increases mouse life span. Strategies that conserve cellular NAD^+ may reprogram dysfunctional SCs and improve life span in mammals.

In adults, tissue homeostasis is highly dependent on stem cell (SC) function. Adult SCs are not only essential in continuously proliferating tissues (like the hematopoietic, intestinal, and skin systems) but also in normally quiescent tissues (such as skeletal muscle and the brain) that require regeneration after damage or exposure to disease (*1*). Aging is accompanied by a decline in adult SC function, termed SC senescence, which leads to the loss of tissue homeostasis and regenerative capacity (*2*, *3*).

Homeostasis and regeneration of skeletal muscle depend on normally quiescent muscle SCs (MuSCs), which are activated upon muscle damage to expand and give rise to differentiated myogenic cells that regenerate damaged muscle fibers (*4*, *5*). These responses are blunted in aged muscle, probably because of the reduced number and function of MuSCs (*6*–*8*). In aging, MuSC dysfunction may be caused by extrinsic signals (*9*, *10*), intrinsic cellular senescence signaling pathways (*11*), or both. One general regulator of cellular senescence, cyclin-dependent kinase inhibitor 2A (CDKN2A, also known as $p16^{INK4A}$), shows increased expression in geriatric MuSCs, which causes permanent cell cycle withdrawal and senescence of MuSCs in very old mice (28 to 32 months of age) (*11*). However, reductions in MuSC number and function can already be observed before this stage (*6*, *11*), indicating that MuSC senescence may be initiated at an earlier time point. Pre-geriatric mice, approximately 2 years old, can exhibit features of MuSC senescence (*8*, *12*–*15*). However, the early mechanisms that instigate MuSC senescence are still largely unknown.

One of the hallmarks of organismal aging is the appearance of mitochondrial dysfunction (*2*, *3*). Induced by calorie-dense diets or aging, mitochondrial dysfunction can result from depletion of the oxidized form of nicotinamide adenine dinucleotide (NAD^+), whereas NAD^+ repletion, with precursors such as nicotinamide riboside (NR), can reverse this process (*16*–*20*). SCs are thought to rely predominantly on glycolysis for energy, a process that would reduce cellular concentrations of NAD^+ (*21*). Mitochondrial function is linked to SC maintenance and activation (*22*–*25*), yet its role in senescence is unknown.

Mitochondrial dysfunction is a biomarker of MuSC senescence

To identify the role of mitochondrial function in SCs, we compared MuSCs from young and aged mice. For the purpose of identifying the principal mechanisms that initiate MuSC senescence, we examined publically available MuSC gene expression data sets from young (~3 months) and aged (~24 months) mice using gene set enrichment analysis [GSEA; Gene Expression Omnibus (GEO) accession numbers GSE47177 (*14*), GSE47104 (*12*), and GSE47401 (*8*)]. Enrichment scores of data sets from young versus aged mice revealed up-regulation of senescence pathways and down-regulation of cell cycle pathways with age (Fig. 1A, tables S1 to S3, and fig. S1, A and B). This finding is consistent with the idea that irreversible cell cycle arrest is a primary marker of cellular senescence (*2*, *3*). In all three data sets, tricarboxylic acid (TCA) cycle and oxidative phosphorylation (OXPHOS) pathways were among the most down-regulated pathways in aged MuSCs (Fig. 1A, tables S1 to S3, and fig. S1, A and B). Analysis of gene ontology terms that were significantly (GSEA; family-wise error rate $P < 0.05$) down-regulated in aged MuSCs further demonstrated links to mitochondrial function (fig. S1C). Genes that were commonly down-regulated during aging showed a substantial overlap (113 genes; 11.59%) with mitochondrial genes (*26*) (Fig. 1B and table S4), in contrast to the minimal overlap (11 genes; 1.92%) among commonly up-regulated genes and mitochondrial genes (fig. S1D and table S4). Among the 113 down-regulated mitochondrial genes in aged MuSCs, 41.6% were related to the TCA cycle and OXPHOS (fig. S1E), which is higher than their percent composition of the whole mitochondrial proteome (~14%) (*27*, *28*). This indicates a dominant decline in expression of mitochondrial respiratory genes in aged MuSCs. The reduction in mitochondrial OXPHOS and TCA cycle genes was consistent for all independent data sets (fig. S1, F and G). We isolated primary aged and young MuSCs and confirmed reduced abundance of OXPHOS and TCA cycle transcripts (Fig. 1C), as well as reduced oxidative respiration rates in both freshly isolated (Fig. 1D) and cultured MuSCs (fig. S1H). MuSC mitochondrial dysfunction in aged mice was further confirmed by the loss of mitochondrial membrane potential (Fig. 1E) and a reduction in cellular adenosine triphosphate (ATP) concentrations (Fig. 1F). Several important markers and regulators of the mitochondrial unfolded protein response (UPR^{mt}), a stress-response pathway that mediates adaptations in mitochondrial content and function, were down-regulated in aged MuSCs (fig. S1F and Fig. 1G). Despite the absence of consistent changes in the CDKN2A (fig. S1I and table S4) or mitogen-activated protein kinase 14 (MAPK14, also known as p38) pathways (table S4), previously reported to regulate MuSC senescence, expression of cell cycle genes was decreased and expression of genes encoding the senescent proinflammatory secretome was increased (fig. S1, I to K). The reduction in cell cycle signaling was accompanied by increased expression of genes in the cyclin-dependent kinase inhibitor 1 (CDKN1A; also known as $p21^{CIP1}$)–mediated pathway (fig. S1K and table S4), which suggests that early senescence in MuSCs may involve CDKN1A.

NAD^+ repletion improves MuSC function in aged mice

Given the importance of NAD^+ concentrations in the control of mitochondrial function (*16*, *29*), we examined the potential of NAD^+ repletion to improve MuSC numbers and muscle function in aged mice. Amounts of NAD^+ in freshly isolated MuSCs were lower in those isolated from aged mice, and 6 weeks of NR treatment increased NAD^+ concentration in MuSCs from young and old mice (Fig. 2A). Amounts of NADH (the reduced form of NAD^+) were relatively stable

[1]Laboratory of Integrative and Systems Physiology, École Polytechnique Fédérale de Lausanne (EPFL), 1015 Lausanne, Switzerland. [2]Department of Biology, Institute of Molecular Systems Biology, Eidgenössische Technische Hochschule Zürich (ETHZ), 8093 Zurich, Switzerland. [3]Laboratory of Molecular Biology of Exercise, School of Applied Science, University of Campinas, CEP 13484-350 Limeira, São Paulo, Brazil. [4]Laboratory of Stem Cell Bioengineering, EPFL, 1015 Lausanne, Switzerland. [5]Faculty of Science, University of Zurich, 8057 Zurich, Switzerland. [6]Metabolic Signaling, EPFL, 1015 Lausanne, Switzerland. [7]Interdisciplinary School of Health Sciences, University of Ottawa Brain and Mind Research Institute, 451 Smyth Road, K1H 8M5 Ottawa, Ontario, Canada.
*Corresponding author. Email: kmenzies@uottawa.ca (K.J.M.); admin.auwerx@epfl.ch (J.A.)

(fig. S2A). Muscle from aged mice contained fewer MuSCs compared with that of young animals (Fig. 2, B and C, and fig. S2, B and C). However, NR treatment increased MuSC numbers in young and old mice (Fig. 2, B and C, and fig. S2, B and C). The increase in MuSC numbers was confirmed by staining with paired box protein Pax-7 (PAX7), a known MuSC marker (*4*) (Fig. 2D and fig. S2, D and E). In both young and aged mice, the effect of NR did not appear to result from changes in muscle or body mass, as these measures remained comparable among all groups over the short treatment period (fig. S2, F to I). NR treatment also enhances muscle function in aged animals through an independent mechanism acting directly on the muscle fibers (*16*), as was apparent from improvements in maximal running times and distances, along with limb grip strength in aged mice (Fig. 2, E to G). Young animals showed no such changes (fig. S2, J to L).

Impairments in muscle regeneration efficiency have been linked to the decline in MuSC function in aged mice (*6*). We therefore examined the benefits of NR on muscle regeneration with cardiotoxin (CTX)–induced muscle damage (*4*). NR treatment accelerated muscle regeneration in aged and young mice (Fig. 2H and fig. S2M). NR-induced improvements in regeneration were paralleled by increases in PAX7-stained MuSCs in aged mice (Fig. 2I and fig. S2N) but not in young mice (fig. S2, O and P). NAD^+ repletion also improved the stemness of the aged MuSCs, as demonstrated by a reduction in the ratio of myoblast determination protein 1 (MYOD1) and PAX7–double-positive to PAX7-positive myofibers (Fig. 2J and fig. S2Q), as MYOD1 is a transcriptional factor that activates MuSC differentiation. Seven days after CTX-induced damage, aged mice treated with NR exhibited elevated levels of fibers positive for embryonic myosin heavy chain, a protein expressed in fetal and newly regenerating adult muscle fibers (*30*) (Fig. 2K). MuSCs were then transplanted from NR-treated or control aged mice into *mdx* (C57BL/10ScSn-*Dmd*^{mdx}/J) mice (fig. S2R) (a mouse model of Duchenne muscular dystrophy that gradually loses MuSC function in aging due to the strain of continual muscle regeneration). MuSCs isolated from NR-treated donors more effectively replenished the MuSC compartment and stimulated myogenesis of dystrophin-positive myofibers when transplanted into either young or aged *mdx* recipients (fig. S2S and Fig. 2L, respectively). Thus, NR treatment can improve both muscle regeneration and MuSC transplantation efficiency.

The inappropriate accumulation of nonmyogenic fibro-adipogenic progenitors (FAPs) and inflammatory cells has been reported to impair MuSC function and muscle regeneration, especially in aged or chronically damaged muscle, as found in *mdx* mice (*31*). NR treatment largely attenuated increases in FAP numbers 7 days after CTX-induced damage in aged mice but had no effect on FAPs under basal conditions (fig. S2, T to V). This finding is consistent with benefits to FAP clearance in later periods of muscle regeneration (*31*). NR also alleviated macrophage infiltration 7 days after CTX-induced regeneration in aged mice (fig. S2, W and X).

NR prevents MuSC senescence by improving mitochondrial function

To explain the improvements in MuSCs from aged animals after NAD^+ repletion, we examined effects on MuSC senescence. Freshly isolated MuSCs from NR-treated young and aged mice were immunostained for phosphorylation of histone 2A.X at Ser^{139} (γH2AX), a marker of DNA damage (*2*). γH2AX-stained nuclei were more abundant in MuSCs from aged animals, and staining was reduced with NR treatment (Fig. 3, A and B; results for young controls can be found in fig. S3, A and B). The reduction of the nuclear damage response in MuSCs was confirmed by a single-cell gel electrophoresis (comet) assay, a sensitive measure of DNA strand breaks as an indicator of senescence (Fig. 3C), as well as by staining for β-galactosidase (β-Gal), another classical

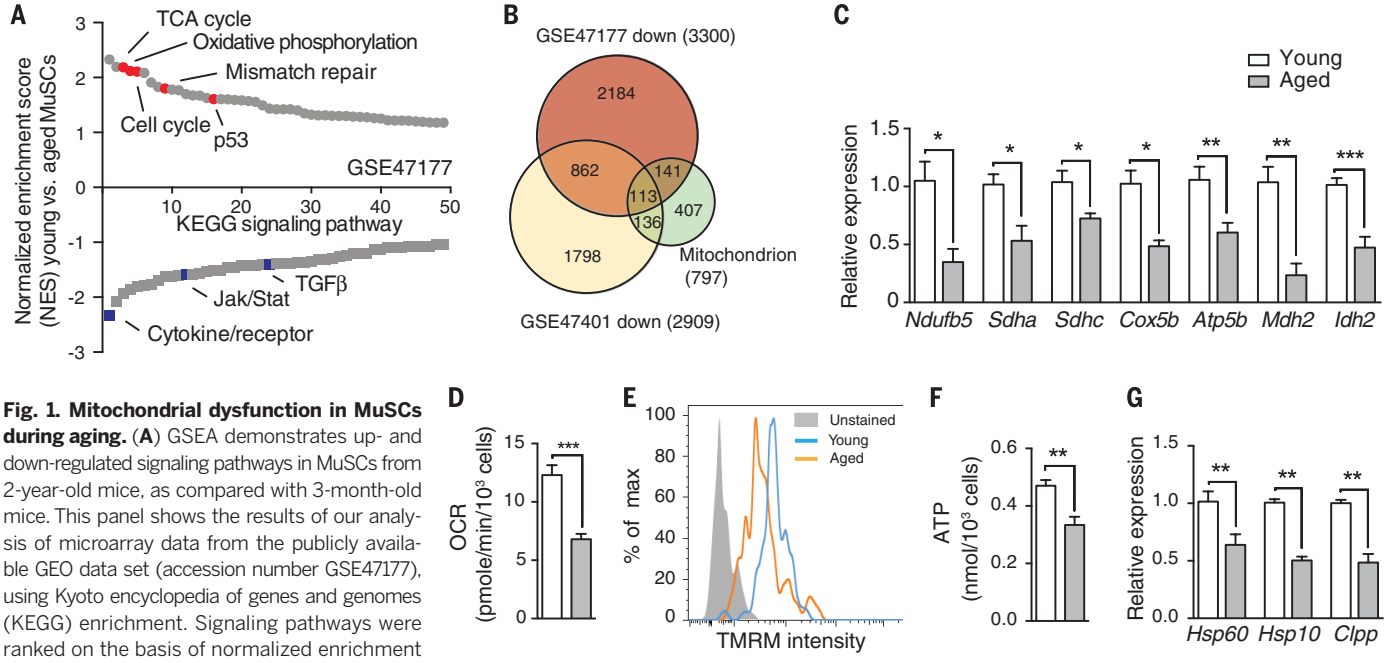

Fig. 1. Mitochondrial dysfunction in MuSCs during aging. (**A**) GSEA demonstrates up- and down-regulated signaling pathways in MuSCs from 2-year-old mice, as compared with 3-month-old mice. This panel shows the results of our analysis of microarray data from the publicly available GEO data set (accession number GSE47177), using Kyoto encyclopedia of genes and genomes (KEGG) enrichment. Signaling pathways were ranked on the basis of normalized enrichment scores (NESs); positive and negative NESs indicate down- or up-regulation, respectively, in aged MuSCs. Specific pathways related to MuSC function are highlighted in red and blue. TGFβ, transforming growth factor–β. (**B**) Area-proportional Venn diagram representing 113 common genes between the significantly down-regulated genes ($P < 0.05$) in MuSC transcriptomes originating from aged mice [GSE47177 and GSE47401 (*12*)] and genes from the human mitochondrial transcriptome (*26*). (**C** to **G**) Young (1 month old) and aged (22 to 24 months old) C57BL/6J mice received a dietary supplement with NR for 6 weeks. (C) Quantitative real-time fluorescence polymerase chain reaction validation of transcriptional changes in mitochondrial genes of freshly sorted MuSCs. (D) Oxygen consumption rate (OCR) in freshly isolated MuSCs after 16 hours of recovery at 37°C. Pmole, picomoles. (E and F) Mitochondrial membrane potential, as measured by a tetramethylrhodamine, methyl ester (TMRM) assay (E) and cellular ATP levels (F) in freshly isolated MuSCs. (G) Relative gene expression for UPR^{mt} genes and cell senescence markers in freshly sorted MuSCs. Data are normalized to *36b4* mRNA transcript levels. All statistical significance was calculated by Student's *t* test. All data are shown as mean ± SEM (error bars). *$P < 0.05$; **$P < 0.01$; ***$P < 0.001$. In (C), (D), (F), and (G), $n = 6$ mice per group; in (E), $n = 3$ mice per group.

senescence marker (*2*) (fig. S3C). A 6-hour NR treatment of late-passage C2C12 myoblasts also reduced the expression of cell senescence and apoptosis markers (*32*) (Fig. 3D). MuSCs isolated from NR-treated aged mice showed enhanced potential to form myogenic colonies (Fig. 3E and fig. S3D). Thus, NR exerts a protective effect against intrinsic MuSC senescence.

Nicotinamide riboside treatment of MuSCs from aged mice reduced abundance of mRNAs encoding CDKN1A and related proinflammatory proteins and increased the expression of cell cycle genes (Fig. 3F). These effects were not observed in nonsenescent MuSCs from young animals (fig. S3E). NR treatment of MuSCs from aged animals increased expression of genes whose products function in the TCA cycle and OXPHOS (Fig. 3G), an effect that was not evident in young animals (fig. S3F). To quantify protein expression levels under different conditions, we applied a new mass spectrometry–based proteomics technique, the sequential windowed acquisition of all theoretical fragment ion mass spectra (SWATH-MS) (*33*), which allows accurate and reproducible protein quantification across sample cohorts. Using this technique, we were able to quantify the expression changes of more than 1100 proteins in MuSCs across the various conditions. The SWATH-MS results show that a significant amount of proteins that function in OXPHOS and in the UPR^{mt} were decreased in MuSCs from aged animals (Fig. 3H and table S6). The overall amount of these same proteins was increased after NR supplementation [two-way analysis of variance (ANOVA) test, $P < 0.05$ (Fig. 3H and table S6)]. Protein immunoblotting of freshly

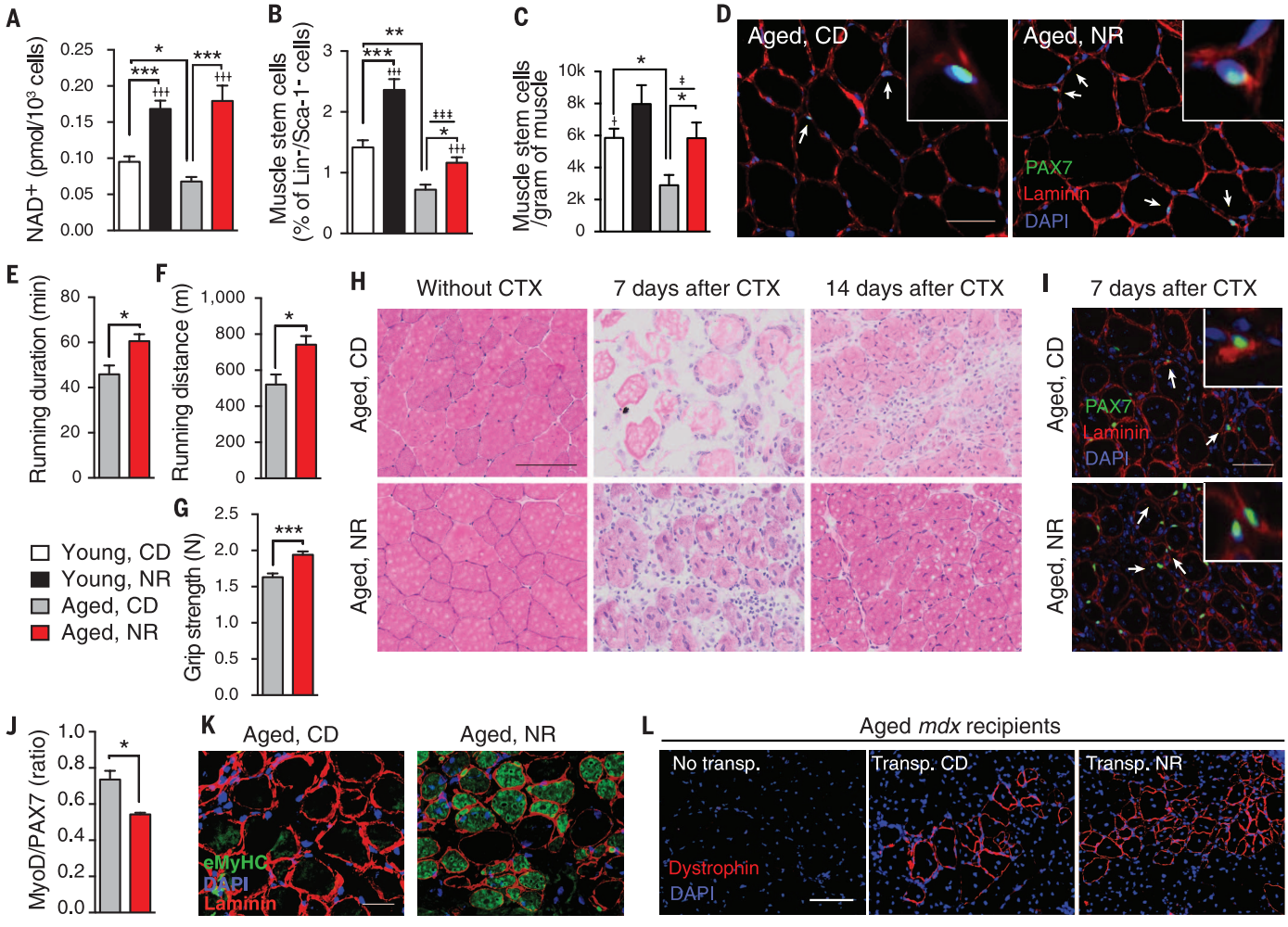

Fig. 2. Improved MuSC numbers and muscle function in NR-treated aged mice. Young (1 month old) and aged (22 to 24 months old) C57BL/6J mice received a chow diet (CD) or a CD supplemented with NR for 6 weeks. All results are compared with those of age-matched mice given a control diet. (**A**) NAD^+ concentrations in freshly isolated MuSCs. (**B** and **C**) Percentage of fluorescence-activated cell sorting (FACS)–quantified $CD34^+$/integrin $\alpha7^+$/Lin^-/Sca-1^- MuSCs relative to the total Lin^-/Sca-1^- cell population (B) or to muscle weight (C). (**D**) Representative images of PAX7- and laminin-immunostained tibialis anterior (TA) muscle. Arrows point to PAX7-positive SCs. Insets (20 μm by 20 μm) show a single MuSC. Scale bar, 50 μm. DAPI, 4′,6-diamidino-2-phenylindole. (**E** to **G**) Comparison of maximal running duration (E), running distance (F), and grip strength (G) in NR-treated aged mice. (**H**) Hematoxylin and eosin (H&E)–stained TA tissue sections from NR-treated aged mice 7 and 14 days after CTX-induced muscle damage. Scale bar, 100 μm. (**I**) Images of PAX7- and laminin-immunostained TA muscle cross sections taken from NR-treated aged mice 7 days after CTX-induced muscle damage. Arrows point to PAX7-positive MuSCs. Insets (20 μm by 20 μm) show a single MuSC. Scale bar, 50 μm. (**J**) Quantification of MYOD1 and PAX7–double positive to PAX7-positive myofibers, performed on sections isolated 7 days after muscle damage in aged mice. (**K**) Newly regenerated muscle fibers stained by embryonic myosin heavy chain (eMyHC) 7 days after muscle damage in aged mice. Scale bar, 50 μm. (**L**) Dystrophin immunostaining of TA muscle sections in aged (16 months old) *mdx* mice 4 weeks after receiving transplantations of MuSCs isolated from control or NR-treated aged C56BL/6J donors. Scale bar, 100 μm. All statistical significance was calculated by Student's *t* test or two-way ANOVA. All data are shown as mean ± SEM (error bars). *$P < 0.05$; **$P < 0.01$; ***$P < 0.001$. Main effects for treatment or age are denoted with † or ‡ symbols, respectively. † or ‡, $P < 0.05$; ††† or ‡‡‡, $P < 0.001$. In (A), $n = 6$ mice per group; in (B) to (D) and (H) to (K), $n = 3$ to 6 mice per group; in (E) to (G), $n = 10$ mice fed the control diet and 7 NR-treated mice; in (L), $n = 12$ donor mice and 3 recipient mice for each treatment. For (E) to (J), corresponding young control data can be found in fig. S2, J to O, respectively.

isolated MuSCs from aged animals confirmed increased expression of proteins related to cell cycle and senescence that could not be detected by SWATH-MS (Fig. 3I).

Muscle SCs from aged mice treated with NR exhibited increases in oxidative respiration (Fig. 3, J and K). NR-treated MuSCs from aged animals also showed increased mitochondrial membrane potential (Fig. 3L and fig. S3G) and increased abundance of ATP (Fig. 3M). To test whether this protective effect of NR on MuSC senescence relies on mitochondrial function, we created a tamoxifen-inducible sirtuin-1 (SIRT1) MuSC-specific knockout mouse (SIRT1$^{MuSC-/-}$) by crossing SIRT1$^{flox/flox}$ mice with the Pax7^{creER} strain. SIRT1 is a NAD$^+$-dependent deacetylase that increases mitochondrial biogenesis (*16*). The beneficial effect of NR on muscle regeneration after CTX injection appeared to be attenuated in SIRT1$^{MuSC-/-}$ mice (Fig. 3N). Supporting this qualitative observation, the act of knocking out SIRT1 in MuSCs blocked the beneficial effects of NR on MuSC activation (Fig. 3, O to Q) and senescence (Fig. 3R and fig. S3H) 7 days after regeneration. These data indicate that NR inhibits MuSC senescence by improving mitochondrial function in a SIRT1-dependent manner. This finding is consistent with a report linking activation of FOXO3, a SIRT1 target, to improved mitochondrial metabolism in hematopoietic SCs (*34*).

Rejuvenating MuSCs by activating the UPR^{mt} and prohibitin pathways

We further explored how UPR^{mt} might regulate senescence by examining the role of prohibitins, a family of stress-response proteins. Prohibitins sense mitochondrial stress and modulate senescence in fibroblasts in mammals (*35*), maintain replicative life span in yeast (*36*), and promote longevity in worms (*37*), animals that lack adult SCs. Expression of the prohibitins *Phb* and *Phb2* was reduced in the bioinformatics analysis (fig. S1F),

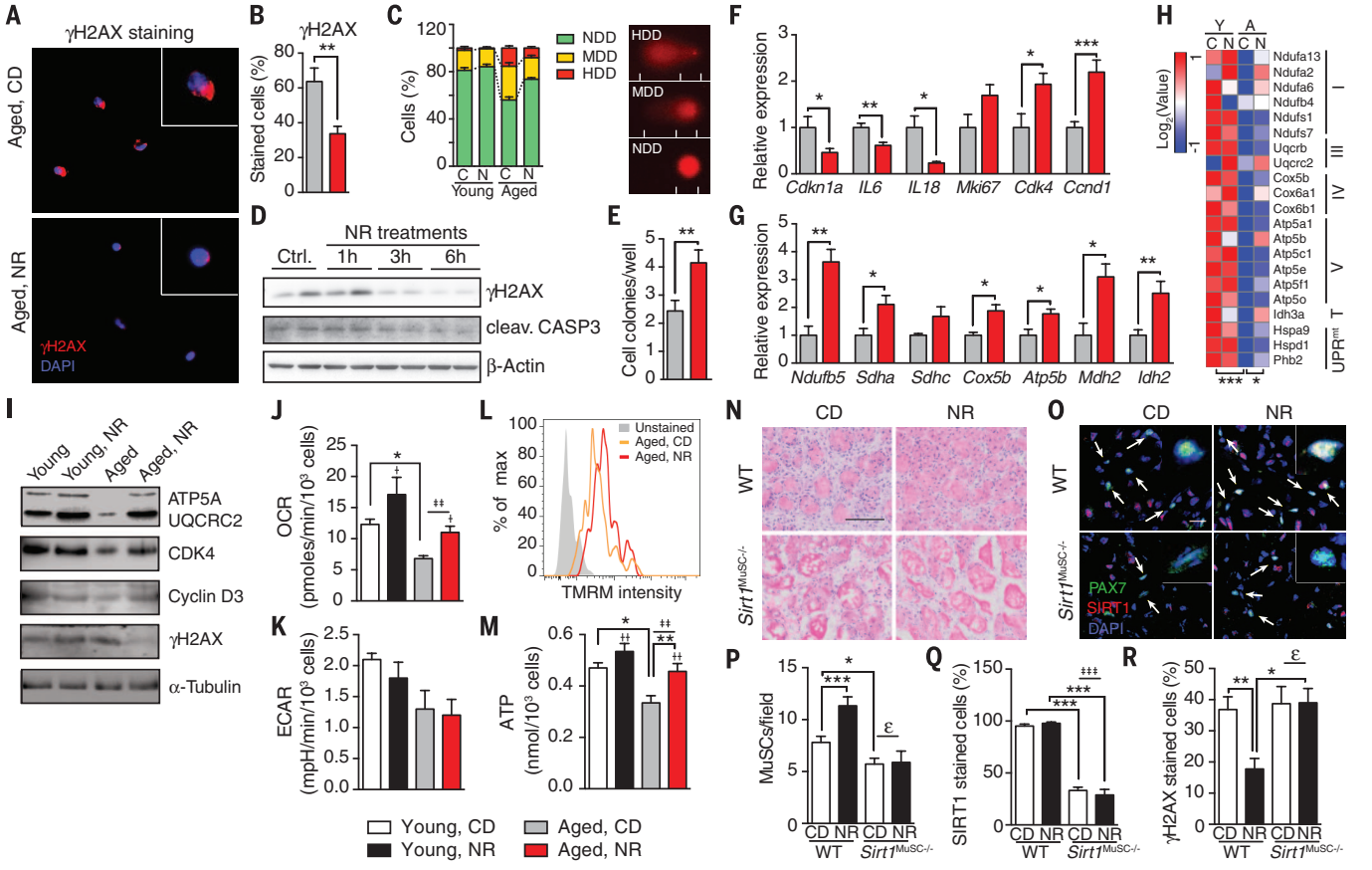

Fig. 3. NR treatment prevents MuSC senescence and improves mitochondrial function. Aged (22 to 24 months old) C57BL/6J mice or 8-month-old SIRT1$^{MuSC-/-}$ mice received a dietary supplement with NR for 6 weeks. All isolated MuSCs were freshly FACS sorted for assay. Most comparative data from young mice (1 month old) are presented in fig. S3. (**A** and **B**) Immunostaining (A) and quantification (B) of γH2AX staining in freshly sorted MuSCs from aged mice. Insets (20 μm by 20 μm) show single MuSCs. (**C**) Single-cell gel electrophoresis (comet) assay of MuSCs from aged mice. C, chow diet; N, NR treated; NDD, nondamaged DNA; MDD, moderately damaged DNA; HDD, heavily damaged DNA. (**D**) Proteins levels in C2C12 myoblasts after NR treatment for 1, 3, or 6 hours. (**E**) Colony-formation ability assay in isolated MuSCs. (**F** and **G**) Quantification of transcript expression for cell cycle and inflammatory secretome genes (F) or OXPHOS and TCA cycle genes (G) in MuSCs. (**H**) Abundance of proteins from MuSCs of young (Y) and aged (A) mice fed with a chow (C) or NR (N) diet. Protein abundances were calculated using the intensities of peptides detected in the SWATH-MS maps. Roman numerals indicate corresponding OXPHOS complexes. T, TCA cycle. (**I**) Protein levels in MuSCs. (**J** and **K**) OCR (J) and extracellular acidification rate (ECAR) (K), in MuSCs after 16 hours of recovery at 37°C. (**L**) Mitochondrial membrane potential, as measured by a TMRM assay in MuSCs. (**M**) Cellular ATP concentration in MuSCs. (**N**) H&E stained TA muscle from wild-type (WT) or SIRT1$^{MuSC-/-}$ mice 7 days after CTX-induced muscle damage. Scale bar, 100 μm. (**O** to **Q**) Representative images (O) and quantification of PAX7-positive MuSCs in random fields of view (160 μm by 160 μm) (P) and the percentage of SIRT1-positive MuSCs (Q) in immunostained TA 7 days after CTX-induced muscle damage. Arrows in (O) point to PAX7-positive MuSCs. Insets (20 μm by 20 μm) show a single MuSC. Scale bar, 50 μm. (**R**) Quantification of γH2AX-positive MuSCs in immunostained TA 7 days after CTX-induced muscle damage. All statistical significance was calculated by Student's *t* test or two-way ANOVA. All data are represented as mean ± SEM (error bars). **P* < 0.05; ***P* < 0.01; ****P* < 0.001. Main effects for treatment or age are denoted as † or ‡, respectively, with interactions denoted as ε. † or ‡, *P* < 0.05; †† or ‡‡, *P* < 0.01; ††† or ‡‡‡, *P* < 0.001. In (A) to (C) and (N) to (R), *n* = 3 to 6 mice per group; in (E), *n* = 24 repeats per group; in (F) and (G) and (J) to (M), *n* = 6 mice per group; in (H), protein was extracted and pooled from 6 mice in each group. For (A), (B), (E), (F), (G), and (L), corresponding young control data can be found in fig. S3, A, B, D, E, F, and G, respectively.

as well as in freshly isolated aged MuSCs (fig. S4A). The addition of NR increased the expression of prohibitin proteins in C2C12 myoblasts (Fig. 4A) and transcripts in MuSCs of young and aged mice (Fig. 4B and fig. S4B). NR treatment was also shown to increase the expression of prohibitins concurrent to markers of UPR^{mt} and the cell cycle (fig. S4C). Moreover, the overexpression of prohibitins, in the absence of NR, likewise increased UPR^{mt} and cell cycle protein expression (Fig. 4C). Demonstrating the dependency of the NR effect on prohibitins, improvements in UPR^{mt} and cell cycle protein expression were not observed with NR treatment after the knockdown of prohibitins (Fig. 4D and fig. S4D). To confirm the regulation of prohibitins on cell cycle proteins and to explore the effect of prohibitins on MuSC function, *Phb* was depleted in vivo through an intramuscular injection of sh*Phb* lentivirus (PHB and PHB2 are functional only as a heterozygous protein complex) (*38*). Impairment of muscle regeneration and a reduction in MuSC numbers were observed in sh*Phb* lentivirus–injected mice 7 days after CTX-induced muscle regeneration (Fig. 4, E and F). Quantifying these results, *Phb* knockdown is shown to block the NR-induced increase of MuSCs upon regeneration (Fig. 4, G and H). *Phb* knockdown does not induce more MuSC senescence in aged mice but does prevent the beneficial effect of NR on MuSC senescence (Fig. 4I and fig. S4E). Initiation of the UPR^{mt} by thiamphenicol also induced expression of prohibitins and cell cycle genes in C2C12 cells (fig. S4F). These results indicate that NR activates the UPR^{mt} and the prohibitin signaling pathway as it inhibits MuSC senescence.

NR reprograms senescence-prone MuSCs in *mdx* mice

With continuous muscle regeneration, MuSCs in *mdx* mice are abnormally active at a young age, leading to MuSC depletion and dysfunction later in life. As a result, primary MuSCs isolated from 14-week-old *mdx* mice were more intensively and frequently stained with β-Gal and had a larger cell size than those of control mice (Fig. 5A and fig. S5, A and B). Similar to the effect in aged animals, NR treatment of *mdx* mice increased

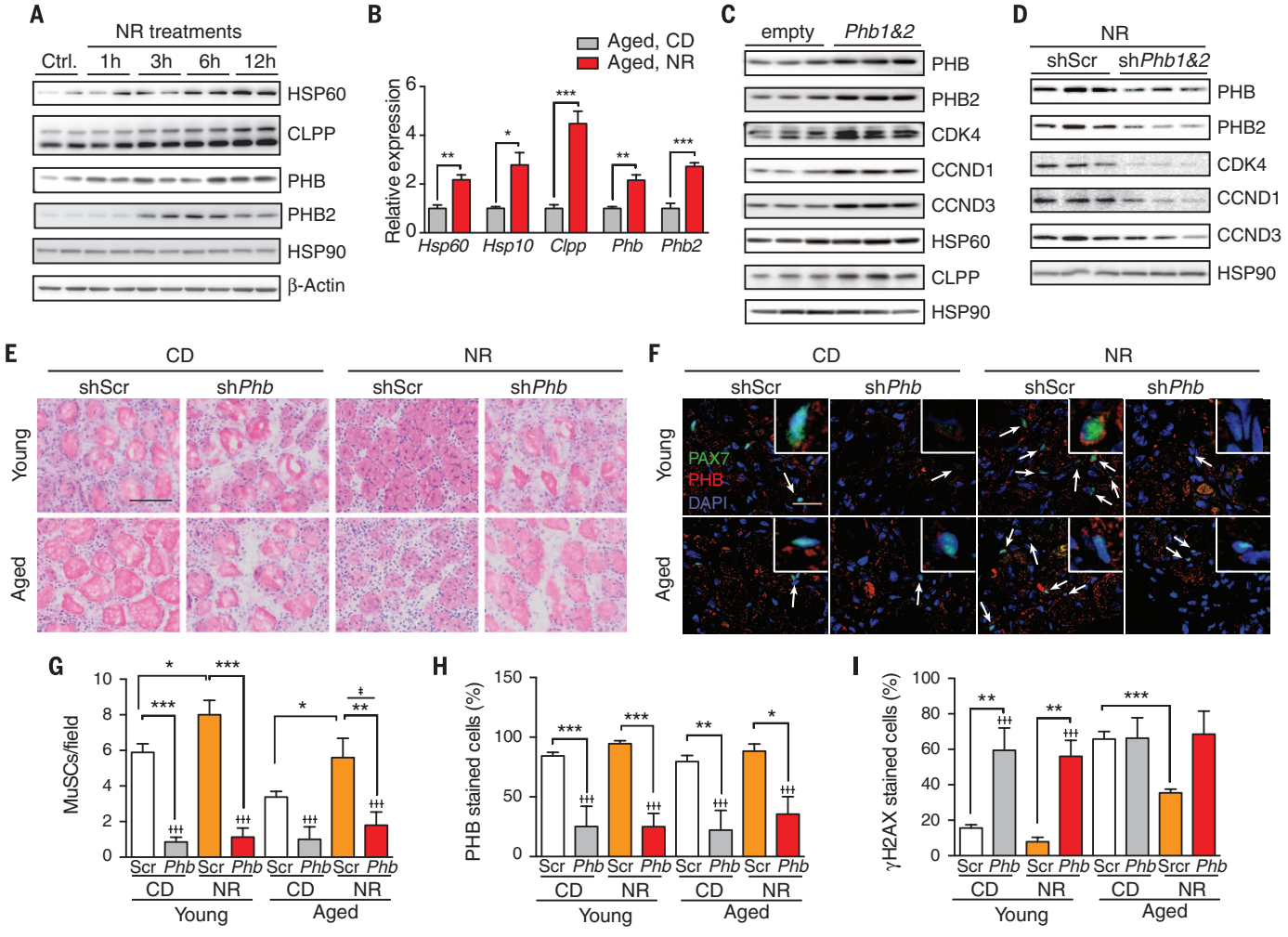

Fig. 4. Effects of NR on prohibitins, UPR^{mt}, and MuSC senescence. (**A**) Expression of HSP60, CLPP, and prohibitins in C2C12 myoblasts upon NR treatment at the indicated time points. (**B**) Quantification of transcript expression for UPR^{mt} and prohibitin genes in MuSCs from aged (22 to 24 months old) C57BL/6J mice after 6 weeks of chow or NR diets. (**C**) Expression of prohibitins and cell cycle proteins in C2C12 myoblasts with the combined overexpression of *Phb* and *Phb2*. (**D**) Expression of prohibitins and cell cycle genes with a 6-hour NR treatment in C2C12 myoblasts after a combined *Phb* and *Phb2* short hairpin RNA knockdown. (**E**) H&E staining of TA muscle in NR-treated or intramuscular sh*Phb* lentivirus–injected C57BL/6J mice 7 days after CTX-induced muscle damage. Scale bar, 100 μm. (**F** to **H**) Representative images (F) and quantification of PAX7-positive MuSCs in randomly chosen fields of view (160 μm by 160 μm) (G) and the percentage of PHB-positive MuSCs (H) in immunostained TA muscle 7 days after CTX-induced muscle damage. Arrows in (F) point to PAX7-positive MuSCs. Insets (20 μm by 20 μm) show a single MuSC. Scale bar, 50 μm. (**I**) Quantification of γH2AX-positive MuSCs in immunostained TA muscle cross sections taken from control and NR-treated mice 7 days after CTX-induced muscle damage. All statistical significance was calculated by Student's *t* test or two-way ANOVA. All data are represented as mean ± SEM (error bars). *$P < 0.05$; **$P < 0.01$; ***$P < 0.001$. Main effects for treatment or *Phb* knockdown are denoted as † or ‡, respectively. † or ‡, $P < 0.05$; ††† or ‡‡‡, $P < 0.001$. In (B), $n = 6$ mice per group; in (E) to (I), $n = 3$ mice per group. For (B), corresponding young control data can be found in fig. S4B.

MuSC numbers by a factor of ~1.8 in vivo (Fig. 5, B to D, and fig. S5, C and D), as also confirmed by PAX7 immunostaining (fig. S5E). Along with the increase in MuSCs, there was an increase in regenerated muscle fibers after NR treatment (Fig. 5E and fig. S5F). We extended this analysis by examining the self-renewal capacity of MuSCs in *mdx* mice. The cellular redox ratio decreases as MuSCs differentiate (*39*), which can be detected by an increase in 450-nm autofluorescence (*40*). In line with NR increasing the number of MuSCs in *mdx* mice, we found reduced autofluorescence from MuSCs isolated from these animals (Fig. 5, F to H). We performed β-Gal staining on primary MuSCs that had been isolated from *mdx* mice with or without NR treatment in vivo and then further cultured with or without NR in vitro. MuSCs isolated from NR-treated mice were less prone to senescence (Fig. 5I and fig. S5G). When MuSCs isolated from control *mdx* mice were treated with NR in vitro, there was also a reduction in senescence (Fig. 5I and fig. S5G). The inhibition of MuSC senescence in NR-treated *mdx* mice was confirmed by the attenuation of γH2AX and cleaved caspase-3 immunostaining (Fig. 5J). To evaluate MuSC function, CTX-induced muscle regeneration was examined in NR-treated *mdx* mice. Consistent with the prevention of MuSC senescence, muscle regeneration was improved with NR in both aged (Fig. 5K and fig. S5H) and young *mdx* mice (fig. S5I). We also examined the effect of NR on the FAP population and muscle regeneration in *mdx* mice. NR treatment increased MuSCs and reduced FAP numbers in basal conditions and 7 days after CTX-induced damage (fig. S5, J to L). Abnormal activation of FAPs in *mdx* mice contributes to fibrosis (*31*). *mdx* mice treated with CTX and then exposed to NR showed lower levels of macrophage infiltration 7 days after damage (fig. S5, M and N). Hence, our results indicate a beneficial effect of NR on MuSC function and regeneration in *mdx* mice.

NR attenuates senescence of neural and melanocyte SCs and increases mouse life span

Aging is accompanied by a decline in the number and function of neural SCs (NSCs) (*23*) and melanocyte SCs (McSCs) (*41*). Therefore, to examine the generalized importance of NAD^+ homeostasis in somatic SCs, we assessed the effect of NR in NSCs from aged mice. NR increased proliferation, as shown by 5-ethynyl-2-deoxyuridine (EdU) and

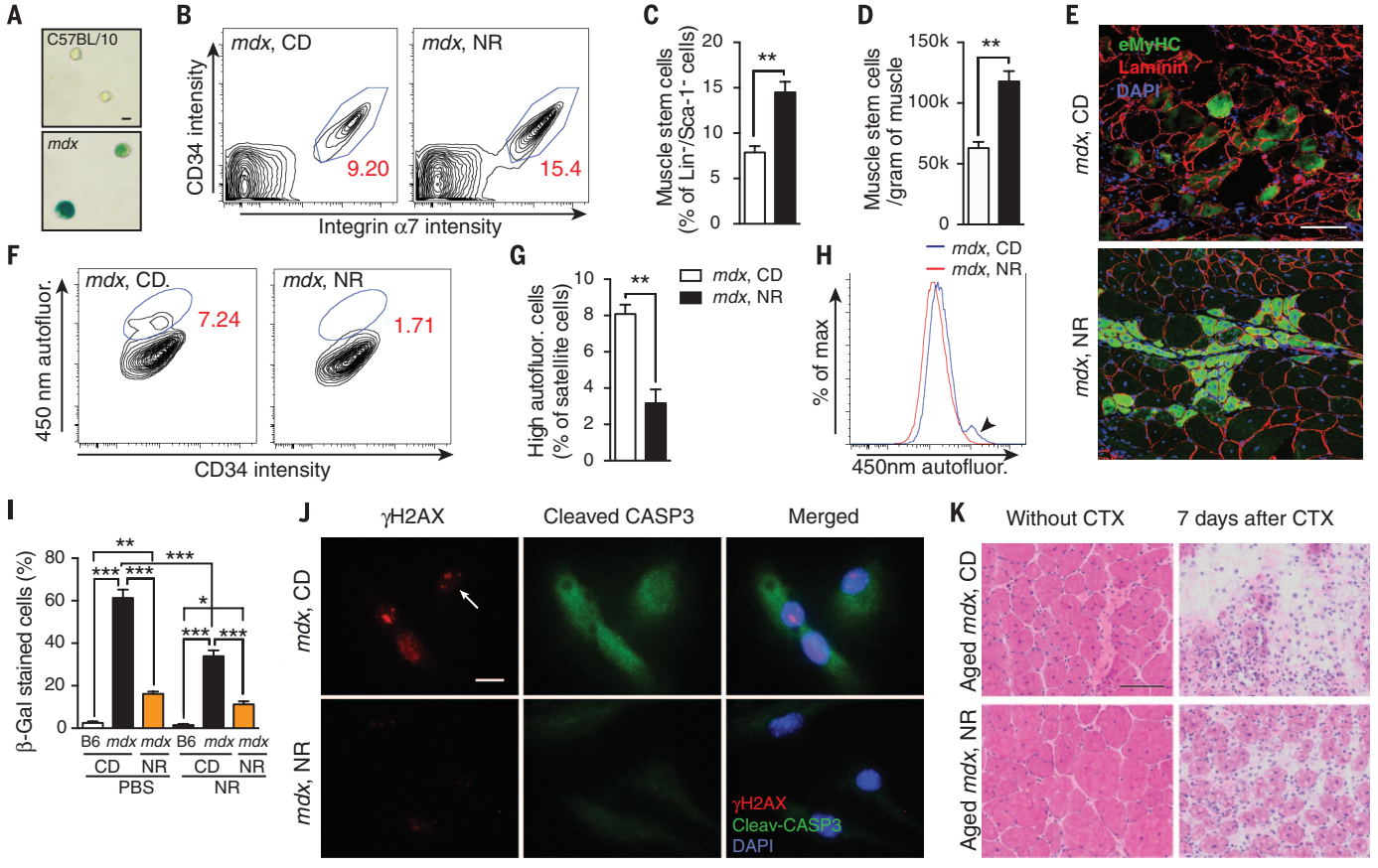

Fig. 5. Increased SC number and function in NR-treated *mdx* mice. *mdx* mice received a dietary supplement with NR for 10 weeks. All results were compared with those of *mdx* mice given a control diet. (**A**) β-Gal staining of MuSCs isolated from C57BL/10SnJ or *mdx* mice and cultured in vitro for three generations. Scale bar, 10 μm. (**B** to **D**) FACS contour plots of Sca-1$^-$/Lin$^-$ cells isolated from muscle. Percentages of the CD34$^+$/integrin α7$^+$/Lin$^-$/Sca-1$^-$ MuSC populations are noted in red in the contour plots (B) and are quantified relative to the total Lin$^-$/Sca-1$^-$ cell population (C) or muscle weight (D). (**E**) Immunostaining of eMyHC$^+$ fibers in tissue sections of NR-treated *mdx* mice 7 days after CTX-induced muscle damage. Scale bar, 100 μm. (**F** to **H**) FACS contour plots (F), quantification (G), and distribution (H) of MuSC autofluorescence as a measure of the relative NAD(P)H concentration (where NADPH is the reduced form of nicotinamide adenine dinucleotide phosphate) upon ultraviolet light excitation. Autofluorescence emission was detected with a wavelength of 450 nm. The arrowhead in (H) points to the highly autofluorescent SC population. (**I**) Quantification of β-Gal staining of FACS-sorted MuSCs from C57BL/6J (B6 with CD), untreated (*mdx* with CD), or NR-treated *mdx* (*mdx* with NR) mice challenged with phosphate-buffered saline or NR for 6 hours in vitro. (**J**) Immunostaining showing γH2AX and cleaved caspase-3 in MuSCs cultured in vitro for three generations. The arrow points to a γH2AX-positive nucleus. Scale bar, 10 μm. (**K**) H&E staining of tissue sections from NR-treated aged *mdx* mice (16 months old) with 7 days of recovery after CTX-induced muscle damage. Scale bar, 100 μm. All statistical significance was calculated by Student's *t* test or one-way ANOVA. All data are represented as mean ± SEM (error bars). **P* < 0.05; ***P* < 0.01; ****P* < 0.001. In (A) to (H), (J), and (K), *n* = 3 to 5 mice per treated group; in (I), *n* = 3 mice and *n* = 6 in vitro treatments. More than 500 cells were quantified for each condition.

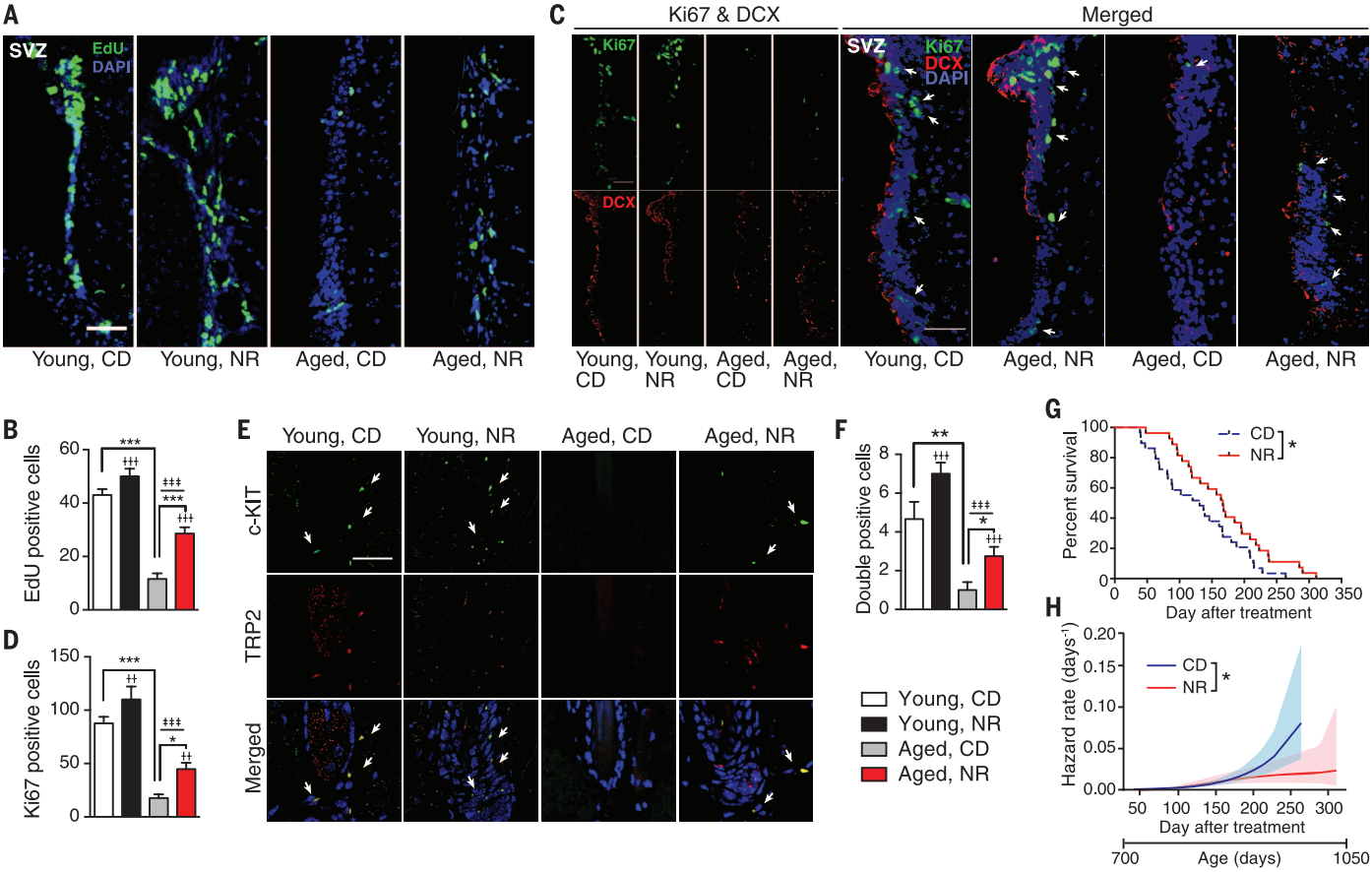

Fig. 6. NR improves NSC and McSC function and increases the life span of aged C57BL/6J mice. Aged (22 to 24 months old) C57BL/6J mice received a dietary supplement with NR for 6 weeks. (**A** and **B**) Representative images (A) and quantification (B) of EdU-positive NSCs in the SVZ from young and aged mice after NR treatment. Scale bar, 50 μm. (**C** and **D**) Representative images (C) and quantification (D) of Ki67- and DCX-positive NSCs in the SVZ, harvested from young and aged mice treated with or without NR. Arrows in (C) point to Ki67-positive NSCs. Scale bar, 50 μm. (**E** and **F**) Representative images (E) and quantification (F) of c-KIT and TRP2 double-positive McSCs in the bulge of hair follicles from dorsal skin, harvested from young and aged mice treated with or without NR. Arrows in (E) point to double-positive McSCs. Scale bar, 50 μm. (**G**) Kaplan-Meier survival curves of control and NR-treated aged mice, with the NR treatment beginning at 2 years (700 days) of age. (**H**) Hazard rate decreased under NR treatment. Individual life spans were collected and used to estimate the hazard function of each population, using numerical differentiation of the Kaplan-Meier survival estimator (solid lines). The shaded areas represent the 95% confidence bands of the true hazard. *P* values were calculated with the use of a Cox proportional hazards model. All statistical significance was calculated by Student's *t* test or two-way ANOVA, except in (G) and (H). All data are represented as mean ± SEM (error bars). $*P < 0.05$; $**P < 0.01$; $***P < 0.001$. Main effects for treatment or age are denoted as † or ‡, respectively. †† or ‡‡, $P < 0.01$; ††† or ‡‡‡, $P < 0.001$. In (A) to (F), $n = 6$ mice per group; in (H), $n = 30$ mice per treated group.

antigen K_i-67 (Ki67) staining, and induced neurogenesis, as indicated by doublecortin (DCX) staining, in both the subventricular zone (SVZ) (Fig. 6, A to D) and the dentate gyrus of the hippocampus (fig. S6, A to D) in aged mice. Nicotinamide mononucleotide, another NAD^+ precursor, also has beneficial effects in aged NSCs (*23*). Similarly, NR rescued the decline of McSCs in hair follicles of aged mice, as reflected by increases in mast/stem cell growth factor receptor Kit (c-KIT) and short transient receptor potential channel 2 (TRP2), known McSC markers, in NR-treated aged mice (Fig. 6, E and F). NR treatment of C57BL/6J mice slightly increased life span (chow diet: mean 829 ± 12.0 days; NR treatment: mean 868 ± 12.4 days; $P = 0.034$) (Fig. 6G). The beneficial effect of NR on survival was further confirmed by Cox proportional hazards analysis (Fig. 6H). Although the life span benefit is small, it was obtained with the NR treatment commencing late in life at 24 months, which indicates that aging may partially stem from the dysregulation of general SC NAD^+ homeostasis.

Conclusions

Oxidative stress, potentially introduced by mitochondrial respiration, is thought to be circumvented in SCs by their reliance on glycolysis as a primary energy resource (*42*). However, our study demonstrates that mitochondrial oxidative respiration is important for the functional maintenance of multiple types of adult SCs during aging. In fact, the reduction in cellular NAD^+ pools blunts the adaptive UPR^{mt} pathway (*18*), ultimately leading to a loss of mitochondrial homeostasis with a concurrent reduction in the number and self-renewal capacity of MuSCs. Accordingly, by boosting the MuSC concentration of NAD^+, proteotoxic stress resistance may be restored due to the activation of the UPR^{mt} pathway, stimulating the prohibitin family of mitochondrial stress sensors and effectors. In turn, this effect will improve mitochondrial homeostasis, protecting MuSCs from senescence and safeguarding muscle function in aged mice (fig. S6E). With the use of a MuSC-specific loss-of-function model for *Sirt1*, an essential regulator governing mitochondrial homeostasis (*43*), the importance and vital nature of the relationship between the NAD^+-SIRT1 pathway, mitochondrial activity, and MuSC function were unequivocally established in vivo. Furthermore, maintaining healthy mitochondria by replenishing NAD^+ stores seems to have beneficial effects beyond MuSCs and also appears to protect NSC and McSC populations from aging.

Our results demonstrate that the depression of prohibitin signaling, leading to mitochondrial

dysfunction, can be reversed in aging by using a nutritional intervention to boost NAD^+ concentrations in SCs. Additionally, our findings suggest that NAD^+ repletion may be revealed as an attractive strategy for lengthening mammalian life span.

REFERENCES AND NOTES

1. A. J. Wagers, I. L. Weissman, *Cell* **116**, 639–648 (2004).
2. T. Kuilman, C. Michaloglou, W. J. Mooi, D. S. Peeper, *Genes Dev.* **24**, 2463–2479 (2010).
3. C. López-Otín, M. A. Blasco, L. Partridge, M. Serrano, G. Kroemer, *Cell* **153**, 1194–1217 (2013).
4. H. Yin, F. Price, M. A. Rudnicki, *Physiol. Rev.* **93**, 23–67 (2013).
5. M. Tabebordbar, E. T. Wang, A. J. Wagers, *Annu. Rev. Pathol.* **8**, 441–475 (2013).
6. Y. C. Jang, M. Sinha, M. Cerletti, C. Dall'Osso, A. J. Wagers, *Cold Spring Harb. Symp. Quant. Biol.* **76**, 101–111 (2011).
7. C. S. Fry *et al.*, *Nat. Med.* **21**, 76–80 (2015).
8. F. D. Price *et al.*, *Nat. Med.* **20**, 1174–1181 (2014).
9. I. M. Conboy *et al.*, *Nature* **433**, 760–764 (2005).
10. J. V. Chakkalakal, K. M. Jones, M. A. Basson, A. S. Brack, *Nature* **490**, 355–360 (2012).
11. P. Sousa-Victor *et al.*, *Nature* **506**, 316–321 (2014).
12. J. D. Bernet *et al.*, *Nat. Med.* **20**, 265–271 (2014).
13. B. D. Cosgrove *et al.*, *Nat. Med.* **20**, 255–264 (2014).
14. L. Liu *et al.*, *Cell Reports* **4**, 189–204 (2013).
15. M. T. Tierney *et al.*, *Nat. Med.* **20**, 1182–1186 (2014).
16. C. Cantó *et al.*, *Cell Metab.* **15**, 838–847 (2012).
17. E. Pirinen *et al.*, *Cell Metab.* **19**, 1034–1041 (2014).
18. L. Mouchiroud *et al.*, *Cell* **154**, 430–441 (2013).
19. J. Yoshino, K. F. Mills, M. J. Yoon, S. Imai, *Cell Metab.* **14**, 528–536 (2011).
20. A. P. Gomes *et al.*, *Cell* **155**, 1624–1638 (2013).
21. K. Ito, T. Suda, *Nat. Rev. Mol. Cell Biol.* **15**, 243–256 (2014).
22. M. Cerletti, Y. C. Jang, L. W. Finley, M. C. Haigis, A. J. Wagers, *Cell Stem Cell* **10**, 515–519 (2012).
23. L. R. Stein, S. Imai, *EMBO J.* **33**, 1321–1340 (2014).
24. P. Katajisto *et al.*, *Science* **348**, 340–343 (2015).
25. J. G. Ryall *et al.*, *Cell Stem Cell* **16**, 171–183 (2015).
26. T. R. Mercer *et al.*, *Cell* **146**, 645–658 (2011).
27. A. Sickmann *et al.*, *Proc. Natl. Acad. Sci. U.S.A.* **100**, 13207–13212 (2003).
28. D. J. Pagliarini *et al.*, *Cell* **134**, 112–123 (2008).
29. R. H. Houtkooper, C. Cantó, R. J. Wanders, J. Auwerx, *Endocr. Rev.* **31**, 194–223 (2010).
30. S. Sartore, L. Gorza, S. Schiaffino, *Nature* **298**, 294–296 (1982).
31. D. R. Lemos *et al.*, *Nat. Med.* **21**, 786–794 (2015).
32. E. Hara *et al.*, *Mol. Cell. Biol.* **16**, 859–867 (1996).
33. L. C. Gillet *et al.*, *Mol. Cell. Proteomics* **11**, O111.016717 (2012).
34. P. Rimmelé *et al.*, *EMBO Rep.* **16**, 1164–1176 (2015).
35. P. J. Coates *et al.*, *Exp. Cell Res.* **265**, 262–273 (2001).
36. P. J. Coates, D. J. Jamieson, K. Smart, A. R. Prescott, P. A. Hall, *Curr. Biol.* **7**, 607–610 (1997).
37. M. Artal-Sanz, N. Tavernarakis, *Nature* **461**, 793–797 (2009).
38. C. Osman, C. Merkwirth, T. Langer, *J. Cell Sci.* **122**, 3823–3830 (2009).
39. M. Fulco *et al.*, *Mol. Cell* **12**, 51–62 (2003).
40. K. P. Quinn *et al.*, *Sci. Rep.* **3**, 3432 (2013).
41. E. K. Nishimura, S. R. Granter, D. E. Fisher, *Science* **307**, 720–724 (2005).
42. C. D. Folmes, P. P. Dzeja, T. J. Nelson, A. Terzic, *Cell Stem Cell* **11**, 596–606 (2012).
43. C. Cantó, K. J. Menzies, J. Auwerx, *Cell Metab.* **22**, 31–53 (2015).

ACKNOWLEDGMENTS

H.Z., D.R., K.J.M., J.A., and the EPFL have filed a provisional patent application on the use of NAD boosting to enhance SC function. We thank T. Langer for sharing the *Phb* plasmids; S. Wang and M. Knobloch for technical help in McSC and NSC experiments; H. Li, L. Mouchiroud, P. Moral Quiros, and all members of the Auwerx and Schoonjans groups for helpful discussions; and the EPFL histology and flow cytometry core facilities for technical assistance. H.Z. is the recipient of a doctoral scholarship from the China Scholarship Council and a fellowship from CARIGEST SA. D.D. was supported by a fellowship from Associazione Italiana per la Ricerca sul Cancro. K.J.M. is supported by the University of Ottawa and the Heart and Stroke Foundation of Canada. J.A. is the Nestlé Chair in Energy Metabolism, and his research is supported by EPFL, the NIH (grant R01AG043930), Krebsforschung Schweiz/SwissCancerLeague (grant KFS-3082-02-2013), Systems X (grant SySX.ch 2013/153), and the Swiss National Science Foundation (grant 31003A-140780).

SUPPLEMENTARY MATERIALS

www.sciencemag.org/content/352/6292/1436/suppl/DC1
Materials and Methods
Figs. S1 to S6
Tables S1 to S6
References (*44*–*54*)

16 January 2016; accepted 13 April 2016
Published online 28 April 2016
10.1126/science.aaf2693

REPORTS

MOLECULAR JUNCTIONS

Covalently bonded single-molecule junctions with stable and reversible photoswitched conductivity

Chuancheng Jia,[1]* Agostino Migliore,[2]* Na Xin,[1]* Shaoyun Huang,[3]* Jinying Wang,[1] Qi Yang,[3] Shuopei Wang,[4] Hongliang Chen,[1] Duoming Wang,[4] Boyong Feng,[3] Zhirong Liu,[1] Guangyu Zhang,[4] Da-Hui Qu,[5] He Tian,[5] Mark A. Ratner,[6] H. Q. Xu,[3]† Abraham Nitzan,[7,8]† Xuefeng Guo[1,9]†

Through molecular engineering, single diarylethenes were covalently sandwiched between graphene electrodes to form stable molecular conduction junctions. Our experimental and theoretical studies of these junctions consistently show and interpret reversible conductance photoswitching at room temperature and stochastic switching between different conductive states at low temperature at a single-molecule level. We demonstrate a fully reversible, two-mode, single-molecule electrical switch with unprecedented levels of accuracy (on/off ratio of ~100), stability (over a year), and reproducibility (46 devices with more than 100 cycles for photoswitching and ~10^5 to 10^6 cycles for stochastic switching).

Rapidly growing research in nanoscience has implications for the development of computing devices, solar energy harvesting, chemical sensing (*1*–*4*), photonics and optoelectronics, biomedical electronics [such as cell-chip connections, cyborg cells (*5*), electroceuticals (*6*), and prosthetics], and biofuel cells (*7*). The development of electronic devices based on controllable molecular conduction aims to meet the urgent demand for further device miniaturization on one hand, and the need to effectively interface organic and inorganic materials for biomedical and nanoelectronic applications on the other. To this end, diverse approaches to molecular nanodevices have been proposed and have faced important issues of reproducibility and stability (*8*).

Switches are basic components of almost any electronic device. The manufacturing of reliable molecular switches is a crucial test of the possibility to use molecules as pivotal components of electronic devices. Molecular switches have been intensively investigated for two decades (*9*–*11*), but only a few studies have demonstrated unidirectional switching (namely, irreversible change) in molecular conduction (*12*–*14*), while failing to produce actual (bidirectional) conductance switching. In this work, we demonstrate a reversible molecular electrical switch that consists of a single diarylethene molecule in a junction comprising graphene electrodes.

[1]Beijing National Laboratory for Molecular Sciences, State Key Laboratory for Structural Chemistry of Unstable and Stable Species, College of Chemistry and Molecular Engineering, Peking University, Beijing 100871, P. R. China. [2]Department of Chemistry, Duke University, Durham, NC 27708, USA. [3]Department of Electronics and Key Laboratory for the Physics and Chemistry of Nanodevices, Peking University, Beijing 100871, P. R. China. [4]Institute of Physics, Chinese Academy of Sciences, Beijing 100190, P. R. China. [5]Key Laboratory for Advanced Materials and Institute of Fine Chemicals, East China University of Science and Technology, Shanghai 200237, P. R. China. [6]Department of Chemistry, Northwestern University, Evanston, IL 60208, USA. [7]Department of Chemistry, University of Pennsylvania, Philadelphia, PA 19104-6323, USA. [8]School of Chemistry, Tel Aviv University, Tel Aviv, 69978, Israel. [9]Department of Materials Science and Engineering, College of Engineering, Peking University, Beijing 100871, P. R. China.
*These authors contributed equally to this work. **†Corresponding author. Email: guoxf@pku.edu.cn (X.G.); anitzan@sas.upenn.edu (A.N.); hqxu@pku.edu.cn (H.Q.X.)**

Science

NAD^+ repletion improves mitochondrial and stem cell function and enhances life span in mice

Hongbo Zhang, Dongryeol Ryu, Yibo Wu, Karim Gariani, Xu Wang, Peiling Luan, Davide D'Amico, Eduardo R. Ropelle, Matthias P. Lutolf, Ruedi Aebersold, Kristina Schoonjans, Keir J. Menzies and Johan Auwerx

Science **352** (6292), 1436-1443.
DOI: 10.1126/science.aaf2693originally published online April 28, 2016

A dietary supplement protects aging muscle

The oxidized form of cellular nicotinamide adenine dinucleotide (NAD^+) is critical for mitochondrial function, and its supplementation can lead to increased longevity. Zhang *et al.* found that feeding the NAD^+ precursor nicotinamide riboside (NR) to aging mice protected them from muscle degeneration (see the Perspective by Guarente). NR treatment enhanced muscle function and also protected mice from the loss of muscle stem cells. The treatment was similarly protective of neural and melanocyte stem cells, which may have contributed to the extended life span of the NR-treated animals.

Science, this issue p. 1436; see also p. 1396